Hindawi

Research Article

Development and Characterization of a New Solid Polymer Electrolyte for Supercapacitor Device

Theodore Azemtsop Manfo ⓘD

Department of Electrical and Electronics Engineering, Faculty of Engineering and Architecture, Recep Tayyip Erdogan University, Zihni Derin Campus, Fener Mahallesi, Merkez 53100, RİZE, Turkey

Correspondence should be addressed to Theodore Azemtsop Manfo; azemsouleymane@yahoo.fr

In this study, solid polymer electrolytes (SPEs) are based on methylcellulose (MC) used as a polymer host and sodium iodide (NaI) as a dopant. The SPE films are developed using different contents of ethyl carbonate (EC) as a plasticizer to enhance their properties via a solution casting method. The surface morphology of SPE films is shown using polarized optical microscopy (POM), which indicates the existence of amorphous patches due to the plasticizing effect of EC. The creation of a complex between MC, NaI, and EC was confirmed by Fourier transform infrared (FTIR) spectra. A tiny amount of EC applied to the MC-NaI polymer salt matrix increases the number of charge carriers and improves ionic conductivity. The ionic conductivity of the generated polymer electrolytes is examined using electrochemical impedance spectroscopy (EIS). The high-ion conducting PE of 5.06×10^{-3} S·cm^{-1} was found with the mixture MC + 50 wt% NaI + 10 wt% EC (room temperature). The linear speed voltammetry (LSV) test shows that the optimized polymer electrolyte can withstand decomposition up to 2.5 V. The optimized sample transmission numbers were calculated using a TNM (transference number measurement) approach, and the results show that 99% of the ions contribute to the conductivity, compared to only 1% of the electrons. A solid-state electrical double-layer capacitor (EDLC) was fabricated using the highest ion-conductive polymer electrolyte and graphene oxide (GO)-based electrodes. The galvanostatic charge-discharge (GCD) technique was performed, and the GCD graph shows the behavior of an ideal capacitor with a less Faradic process and a low ESR value. The GO-based cell's columbic efficiency is 100%, and the system delivers the charge for a long duration. The EDLC cell demonstrates outstanding cyclability. The specific capacitance of the EDLC cell incorporated with MC + 50 wt. % NaI + 10 wt. % EC was found to be 154.66 F/g.

1. Introduction

Investigators were promptly inquisitive about the fabrication of polymer electrolytes after Fenton et al. unveiled it in 1973 [1]. Rapid developments and future trends in the demand for batteries and supercapacitors are ultimately causing a surge in the need for polymer electrolytes (PEs). PEs have emerged as the most promising alternatives in the supercapacitor market because they can eliminate leakage, a major safety concern with liquid electrolytes. In addition, PEs are used in many different electrochemical devices such as fuel cells, sensors, and electrochromic devices [2]. Even though it has this important characteristic, it also has other attractive qualities. These include the ability to make very thin layers of plastic, being flexible without getting damaged, and sticking well to electrolytes. However, a lack of liquid diminishes σ, which poses a significant barrier to the development of high-performance battery systems. As a result, many scientists have worked hard throughout the years to increase σ of PEs [3–7].

Gel polymer electrolyte (GPE) is a SPE with strong σ, a low chance of leakage, no harmfulness (not at all like water frameworks), and awesome warm resistance (not at all like combustible organic systems) [8]. SPEs have intrigued analysts due to their beneficial properties for supercapacitors, such as excellent mechanical steadiness and σ (10^{-3}-10^{-2} S/cm) [9]. SPE outflanks ordinary fluid electrolytes in terms of no electrolyte spillage, negligible combustibility, great

adaptability, security, and steady electrode-electrolyte contact [10, 11]. SPE has a strong adhesion function to the electrode surface and lowers the interfacial impedance between the electrolyte and the electrode as a result of these features. Plasticizer-based SPEs for SCs increase ion transport and cell voltage while decreasing equivalent series resistance (ESR). ESR is strongly dependent on the conductivity of the electrolyte and electrodes, as well as other electrolyte material parameters. However, modern SPEs have low σ at RT and high contact resistance [12]. By increasing the amount and mobility of charge carriers (ions) entering the amorphous area, salt doping enhances σ [13]. The creation of novel highly conductive PEs requires a flexible, resilient, and robust polymer as a potential PE [14]. One of the most important variables to examine when trying to understand how the improvement of ionic conductivity occurs through the host matrix is the ionic transport mechanism in PE [15].

PEs are suitable for energy storage systems due to their wide potential window, good thermal stability, and good electrode-electrolyte interface contact. PEs based on synthetic polymers such as polyethylene oxide (PEO), polyvinyl alcohol (PVA), polyvinyl chloride (PVC), and polyvinylidene fluoride (PVDF) have attracted a lot of interest in recent decades. Despite their extensive use, their non-biodegradability can lead to pollution of the environment [16]. To keep the environment sustainable and clean, current research is focusing on producing polyelectrolytes based on natural and environment friendly polymers [16].

Naturally, cellulose is a carbohydrate polymer that is the most abundant biomass material on the planet. Its low cost, degradability, and great thermal stability make it particularly appealing. The use of methyl chloride in cellulose, named methylation, appears as a solution to dissolve cellulose. The methylation will form MC, which can dissolve in water. MC is nonpolluting, affordable, and has suitable film formation characteristics such as clarity and exceptional physical and electrical capabilities [17]. Cations in NaI can coordinate with O_2 atoms in MC via dative linkages. As a benefit in terms of conductivity, the functional groups present in MC, such as C-O-C, O-H, and O-CH_3, have isolated pair electrons that are responsible for ion transport [18]. In addition, the MC polymer has an amorphous structure, exhibiting quite high glass transition temperature (T_g) in the range of 184–200°C [19]. Meanwhile, cellulose-based GPE can provide appealing electrochemical performance due to its natural advantage of numerous hydroxyl groups [20].

Supercapacitors (SCs) have attracted considerable research attention as energy sources because of their high specific power and long cycle life as compared to rechargeable batteries [21]. As the EDLC stores energy through the process of adsorption or desorption or a non-Faradaic mechanism, a large surface area electrode is crucial [22]. The EDLC's performance can be improved either by modification of the electrolytes or electrodes. Current accomplishments have demonstrated that polymer electrolytes (PEs) are appropriate because of their solvent-free, leakage-free, easy formation of thin films, easily manageable, and

common electrochemical windows in comparison to their commercial liquid electrolyte counterparts [23, 24]. Scientists have done a lot of research on using ammonium salts in MC to make better PEs [25, 26], but less attention has been paid to PEs including sodium salts. Sodium is abundant and less expensive than lithium. Also, the materials are very soft which makes it easier to touch and stay connected to other parts in batteries [27]. Aziz et al. [25] created suitable green PEs made of MC and NaI for EDLC. The solution casting approach was used to make green SPEs with different amounts of NaI. The maximum conductivity of the optimized MC-NaI sample was found to be 3.01×10^{-3} S·cm^{-1} for a composition of 50% NaI. The incorporation of NaI into MC enhanced ion contribution up to 0.93. The electrochemical stability potential window was about 1.7 V. The EDLC delivers a high capacitance of 94.7 F/g. Abdullah et al. [28] prepared SPEs using polyvinyl alcohol (PVA) and MC-incorporated NaI salt. The highest value of σ was 1.53×10^{-5} S·cm^{-1} for the composition MC + 50 wt% NaI. Cyriac et al. [29] prepared SPE films via the solution casting technique. The effect of NaI on a polymer blend matrix composed of sodium carboxymethyl cellulose (NaCMC) and PVA was investigated. The results show the highest conductivity of NaCMC/PVA-based SPE film was about 2.52×10^{-3} S·cm^{-1} for 30 wt% NaI. The incorporation of NaI into the NaCMC/PVA matrix has decreased the crystallinity of the SPE film, as confirmed by XRD data. The FTIR approach confirmed the complexation between NaI, NaCMC, and PVA due to the formation of Na$^+$ and -OH groups and hydrogen bonds between the I and -CH groups. The salt incorporation has promoted the number of ions but still shows a decrease in thermal stability. TNM measurements showed that ion species contributed 0.99 in the optimized sample.

For this reason, free-standing PEs made of MC, NaI, and EC with outstanding properties are developed for EDLC. New biopolymer electrolytes (BEs) especially appear to be potential materials for energy storage devices due to their chemical and mechanical stability, high-ionic conductivity, and high power output in the device. The goal of this research is to create solid biodegradable and sustainable PEs composed of pristine MC with exceptional characteristics including high σ (10^{-3}-10^{-2} S·cm^{-1}), a very low electronic conductivity ($t_{ion} \geq 0.99$), and good flexibility and stability via the solution casting method for application in solid-state supercapacitors. The potential of MC-based SPEs will be thoroughly studied using optical, physical, electrochemical, and ionic transport studies. In addition, the optimal PE is identified for EDLC fabrication, and its specific capacity is investigated.

2. Materials and Approaches

To manufacture the SPE films, MC (Mw = 658.7 g·mol^{-1}), NaI (Mw = 40×10^3 g·mol^{-1}), EC (Mw = 88.06 g·mol^{-1}), and double distilled water (DDW) are used without modification. Figure 1 depicts the chemical structure of each substance. Each SPE film was characterized using different approaches as described in the following section.
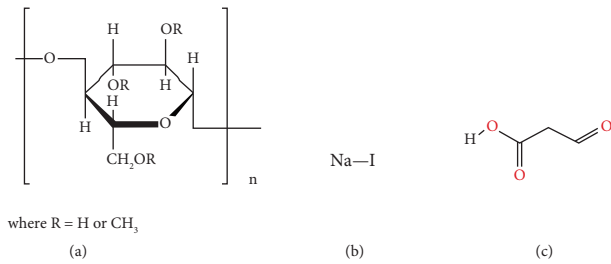
FIGURE 1: Chemical structure of (a) pristine MC, (b) NaI, and (c) EC.

2.1. Polymer Salt Synthesis without Plasticizer.

A chosen amount of 1 g of MC was mixed in 80 ml of DDW and wiggled for a few hours till a completely dissolved solution is obtained at RT. Following that, a predetermined amount of 50 wt. % NaI was introduced to the MC solution and agitated for several hours. Four identical solutions of MC: NaI polymer salt were prepared.

2.2. Polymer Salt Synthesis with Plasticizer.

The four solutions were then doped with different contents of EC ($x = 0$, 10, 20, 30, and 40 wt. %) and stirred for the whole day until transparent homogeneous solutions are obtained. The samples were labeled SPE0, SPE1, SPE2, SPE3, and SPE4, corresponding to 0, 10, 20, 30, and 40 wt% EC, respectively. Following that, each solution was cast into a Petri dish at RT and dried for a week in a desiccator containing silica gel powder. Table 1 summarizes the components of the MC-based SPE samples with their contents. Figure 2 shows the micrograph of the obtained SPE films that were characterized using many methods. The optimal film was used as a separator in the supercapacitor cell as detailed in the following sections.

2.3. Measurements.

All the developed films, pure MC, MC-NaI, and MC-NaI: EC PEs, with various concentrations of EC were characterized using several approaches. The EIS, LSV, TNM, and CV approaches were carried out via the electrochemical workstation over the frequency range of 0.01–1 MHz.

2.3.1. POM Approach.

The morphology of the film surfaces was investigated via the Motic BA310E microscope to evaluate the effect of EC in the MC-NaI polymer salt complex.

2.3.2. FTIR Approach.

Various polymer-ion interactions and specific functional groups contained in SPE films were measured using a Perkin–Elmer FTIR spectrometer (model RX1) at 25°C. This method was also utilized to evaluate the complexity of the relationships among MC, NaI, and EC.

2.3.3. EIS Analysis.

The electrical behavior of the MC-NaI: EC-based SPEs was investigated via the EIS method. This approach measures the impedance between two stainless

TABLE 1: The composition of MC: NaI-based SPE films.

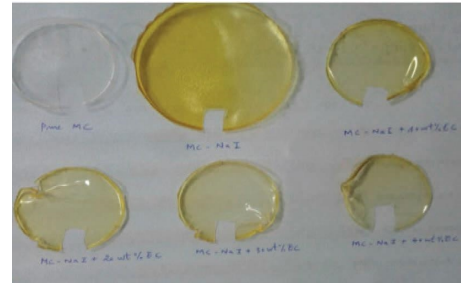| Samples	MC (g)	NaI (wt. %)	EC (wt. %)	EC (g)
SPE0	1	50	0	0
SPE1	1	50	10	0.11
SPE2	1	50	20	0.25
SPE3	1	50	30	0.42
SPE4	1	50	40	0.66

FIGURE 2: Pure MC and MC-based SPE films.

steels (SS), SS/SPE/SS. The resistance value relies on the addition of various concentrations of EC to the MC-NaI polymer salt.

(1) Ionic Conductivity Measurements. The σ value was measured by embedding each PE between two SS electrodes via a sample holder as illustrated in Figure 3. The σ value has been determined using the following equation [30]:

$$\sigma = \frac{d}{R_b \times A}, \tag{1}$$

where R_b is the bulk resistance, A is the section area ($1 \times 1 \, \text{cm}^2$) of the film, and d is the thickness of the film measured with a screw gauge 0–25 mm.

(2) Dielectric Constant. Dielectric constant (ε^*) was measured for each sample using the following equation:

$$\varepsilon^* = \varepsilon' - j\varepsilon'' = \frac{1}{j\omega\varepsilon_0 Z^*}. \tag{2}$$

The complex impedance data at 1 kHz frequency are used to derive the dielectric constant values. Equations (3) and (4) are used to calculate real (ε') and imaginary (ε'') parts of the complex permittivity (ε^*), respectively:

$$\varepsilon' = \frac{Z''}{\left(Z''^2 + Z'^2\right)\omega C_0}, \tag{3}$$

$$\varepsilon'' = \frac{Z'}{\left(Z''^2 + Z'^2\right)\omega C_0}, \tag{4}$$

where Z' and Z'' are real and imaginary parts of impedance spectroscopy (Z^*), ω is the angular frequency ($\omega = 2\pi f$), $C_0 = \varepsilon_0 (A/d)$ is the free space capacitance, and ε_0 is the vacuum permittivity.
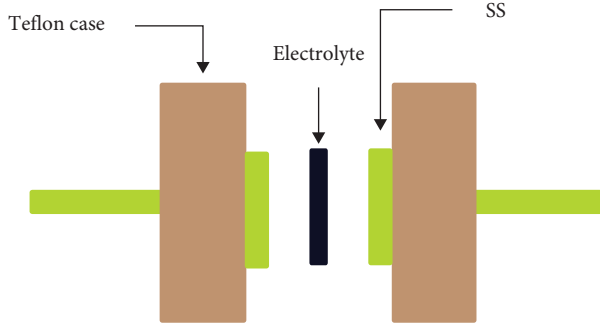
FIGURE 3: The schematic diagram for TNM, LSV, and impedance investigations [30].

(3) Carrier Density and Mobility. Carrier density (n_0) and mobility (μ) were determined using equations (5) and (6), respectively [31]:

$$n_0 = \left[\frac{\sigma_0}{3\varepsilon_0\varepsilon_s'\omega_{10\varepsilon}}\right]^4 \frac{\varepsilon_0\varepsilon_s'KT}{e^2 d^2}, \tag{5}$$

where σ_0 is the dc value of σ at RT, e is the elementary charge, and K and T are Boltzmann constant and thermodynamic temperature, respectively, and the effective value of ε is expressed as $\varepsilon'(\omega_{10\varepsilon}) = 10\varepsilon_s'$ [31].

The μ value is determined via the following relationship [31, 32]:

$$\mu = \frac{\sigma_0}{en_0}. \tag{6}$$

2.3.4. LSV Method. This tool is used to verify the maximum potential voltage of the optimal SPE film. The LSV method can also measure the working electrode current because the potential difference between the electrode and the reference electrode varies linearly with time.

2.3.5. TNM Method. Wagner's polarization method was utilized to evaluate ion contribution in the SPE film. The film is scanned between two stainless steel plates at a constant scan rate, and the current density is recorded over time. Total conductivity can be evaluated through the calculation of the ion transference number (t_{ion}) and electron transference number (t_{elec}) using relationships (7) and (8) shown [33]:

$$t_{\text{ion}} = \frac{I_i - I_{\text{ss}}}{I_i}, \tag{7}$$

$$t_{\text{elec}} = 1 - t_{\text{ion}}, \tag{8}$$

where I_{ss} and I_t are the steady-state and total currents, respectively.

2.4. Preparation of GO. GO material was prepared using the exfoliation approach [34]. GO was synthesized by the mixture of DDW and H_2SO_4 in the proportion 10 : 90 wt%, respectively. Electric wires, connected to both platinum cable and graphite, are first connected to a power supply before being inserted in the prepared solution. The entire system was covered with a paraffin membrane, and a fixed voltage of 4 V was supplied for 5 hours to finish the exfoliation process. The obtained black product was completely supersonicated, cleansed, refined, dehydrated, contained, and then baked at 80°C.

2.5. Manufacturing and Testing of an EDLC

2.5.1. EDLC Fabrication

(1) Electrode Fabrication. The optimal MC-NaI-EC-based SPE film and two GO-based electrodes were utilized to manufacture an EDLC. 1×1 cm^2 area graphite sheets are used as current collectors and coated with GO to make the electrodes. The GO material was obtained by dissolution of P (VDF-HFP) (binder) in a tiny amount of acetone (solvent), mixed up with GO in a ratio of 10 : 90 wt%. The entire slurry is then squashed to make a homogeneous solution. The graphite sheets were then uniformly covered with the GO paste and baked overnight at 80°C.

Conclusively, the high-ion conducting SPE sample was sandwiched between two GO electrodes to make an EDLC. The EDLC is then assembled as illustrated in Figure 4.

2.5.2. Investigation of the EDLC

(1) Cyclic Voltammetry. Cyclic voltammetry (CV) analyzes the nature of charge storage at contact between electrolyte and electrodes, and its output is measured over a set limit of voltage. The CV approach can be used to analyze the nature of the charges stored in the EDLC cells at the interfacial zone between the anodic and cathodic regions [35]. The EDLC was assembled and tested using the CV approach at a fixed scan rate. The capacitance area of the CV graph was determined by applying an integration function within Origin 8.5 software, and C_{sp} of the EDLC was derived using the following subsequent equation:

$$C_{\text{sp}} = \int_{V_1}^{V_2} \frac{I(V)dV}{2mS(V_2 - V_1)}, \tag{9}$$

where m is the GO mass (1.2 mg) and S is the scan rate.

(2) Galvanostatic Charge-Discharge. The GCD approach is experimentally opposed to the CV method where the variations of charges and discharges are observed within a voltage range under a fixed applied current. This tool manifests the actual performance of the cell. The coulomb efficiency was determined via the following relationship:

$$\eta = \frac{\Delta t_D}{\Delta t_C} \times 100\%, \tag{10}$$

where Δt_D is the discharge time and Δt_C is the charge time. The C_{sp} value of the supercapacitor was obtained by exploiting the GCD data via the following equation:
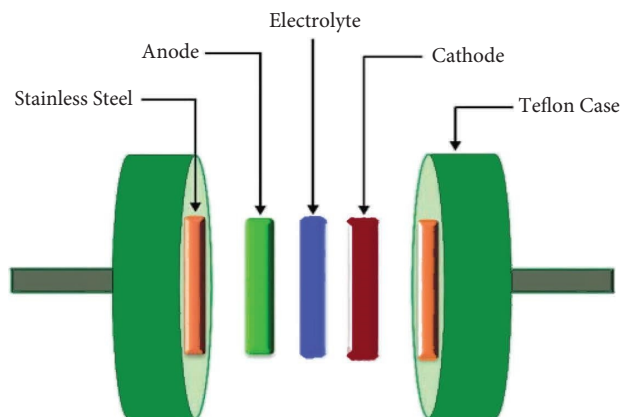
FIGURE 4: Schematic illustration of EDLC for CV, EIS, and GCD measurements [34].

$$C_{sp} = \frac{I}{(dV/dt)m}, \qquad (11)$$

where I is the discharging current and dV/dt is the slope of the discharge curve.

(3) Low Frequency-EIS Approach. This approach is employed to evaluate the value of C_{sp} at lower frequencies. The C_{sp} value of the EDLC is obtained using the following expression:

$$C_{sp} = \frac{-1}{2\pi f Z'' m}, \qquad (12)$$

where f is the frequency.

3. Results and Discussion

3.1. POM Analysis. To comprehend the compatibility between each component of the SPEs, the study of the phase transitions can be monitored using the POM approach. Figure 5 presents the micrographs of pure MC, NaI, EC, MC-NaI, and the optimized MC-NaI: EC-based SPE film. The surface morphology of each SPE film looks uniformly homogeneous with no phase separation. Figure 5(a) shows the surface morphology of pristine MC. It appears that the morphology of MC is compact and an obvious interconnected porous structure is observed. The morphology of the MC sample also reveals traces of scratches and damages, which characterize the substrate-surface state. The scratches and damages appear due to the roughness of the surface of the Petri dish used to prepare the MC film. The structure of the MC film is seen to be weakly ordered. The surface morphology of MC exhibits spherulite and microspores with different sizes dispersed along the surface of the pure film. Prior study has shown that spherulite is associated with the crystalline region, while the dark regions between spherulite interfaces are associated with the amorphous phase [36]. The presence of the spherulites with small amorphous regions between the spherulites in the morphology confirms that MC is semicrystalline. Figures 5(b) and 5(c) show the surface morphology of NaI and EC, respectively. The inclusion of 50

wt. % NaI in the MC matrix has crucially changed the morphology of MC: NaI polymer electrolyte, as shown in Figure 5(e). It has observed a reduction in the size of the MC spherulites and consequently an increase of darker regions upon the incorporation of NaI salt, which suggests an increase in amorphicity. The morphology of the MC: NaI sample is homogeneous and uniform, albeit with varying degrees of roughness from the addition of NaI. It has been shown that salt ions can combine with polymer chains to create complexes, minimizing interactions between hydrogen bonds in the polymer's matrix and increasing the amount of amorphous material [37]. Previous research has postulated that rough surfaces connecting polymer electrolytes act as conduits for ion conduction via the electrolyte [38–40]. In addition, the production of ion pairs, which is unrelated to the ionic conduction process, was described as the emergence of particles on the surface of samples [41–43]. At high salt concentrations, salt can aggregate due to the unsuitability of the integrated salt into the polymer plus the interionic electrostatic bonds. Ion pairs are created when the salt concentration exceeds a certain level, which causes salt to flow to the surface. It is clear from the POM micrograph image that the sample's surface contains tiny white specks. Bhad and Sangawar, who combined PVA with NH$_4$SCN salt, also noted this effect [44]. They discovered that the white particles on the electrolyte surface can act as conduits or paths for proton conduction across the electrolyte. The 10 wt. % EC addition to the MC: NaI matrix has significantly reduced the number of white particles (aggregates) in the morphology of the sample with increased dark regions (Figure 5(e)). The dark regions appear due to the impact of the EC plasticizer resulting in increasing amorphousness in the EC-based SPE film. The reduction in salt aggregation (ion clusters) suggests ion dissociation into the matrix. The ionic dopant NaI is thought to dissociate more quickly in the presence of EC, increasing the dissociation of Na$^+$ toward the MC matrix. According to this technique, EC establishes a network with a reduced path, allowing Na$^+$ to increasingly readily travel through and spread each place. During the conduction phase, weak bonds formed between Na$^+$ and the oxygen atoms of the EC before the Na$^+$ leaped to the C=O of the SPE. The energy threshold was also lowered as a result of the decreased effective hop distance [45]. As a result, the inclusion of EC has changed the sample's optical micrograph, indicating an increase in ionic conduction.

3.2. FTIR Analysis. FTIR approach was performed to investigate the interactions between pristine MC, NaI, and EC. The IR data of NaI, EC, pure MC, polymer salt, and the optimized SPE are seen (Figure 6). The IR spectrum of pure NaI is shown in Figure 6(a). Some absorption peaks are visible at 3428, 3443, 2005, 1987, 1607, 1361, 1082, 776, and 706 cm^{-1}. Figure 6(b) depicts the IR spectrum of pure EC. Some peaks of vibration can be seen clearly at 2996, 1797, 1774, 1559, 1477, 1395, 1156, 1067, 974, 776, and 721 cm^{-1}. Figure 6(c) reveals the IR spectrum of MC. A stretching vibration of O-H at 3428 cm^{-1} and C=C stretch at 1462 cm^{-1} suggested the presence of alcohols and aromatic
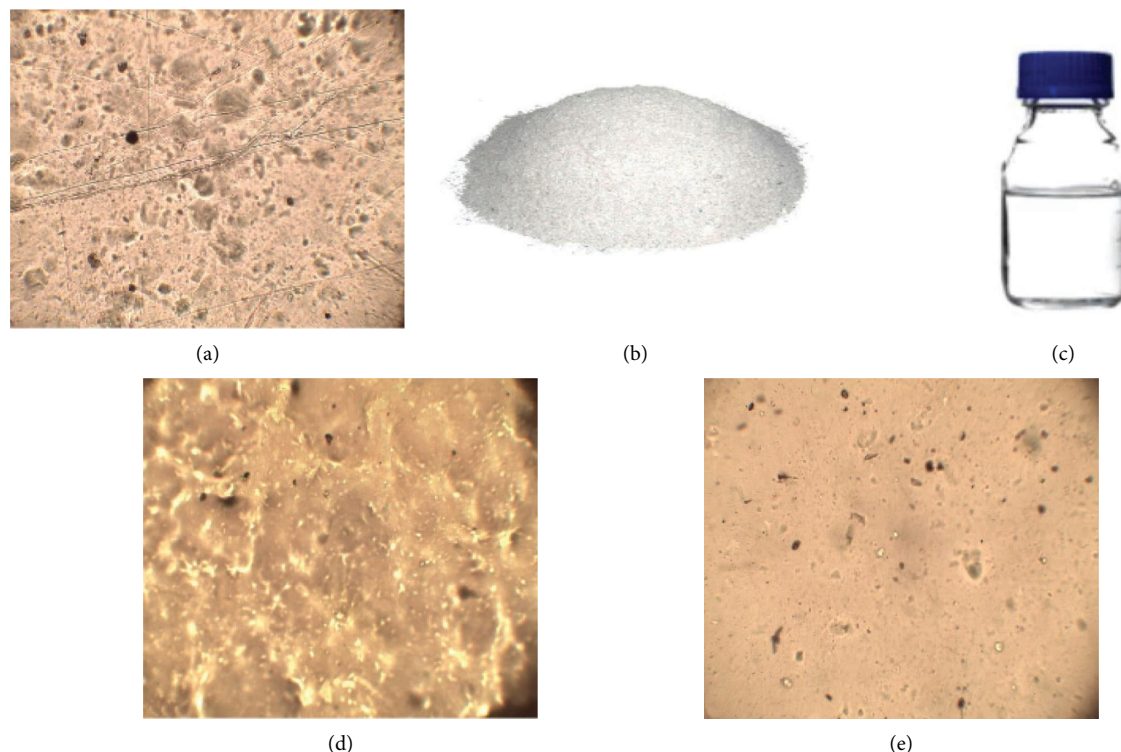
FIGURE 5: Micrographs of (a) pristine MC film, (b) NaI, (c) EC, (d) MC + 50 wt% NaI, and (e) MC + 50 wt% NaI + 10 wt% EC film recorded with ×10 magnifications and a scale bar of 100 μm.
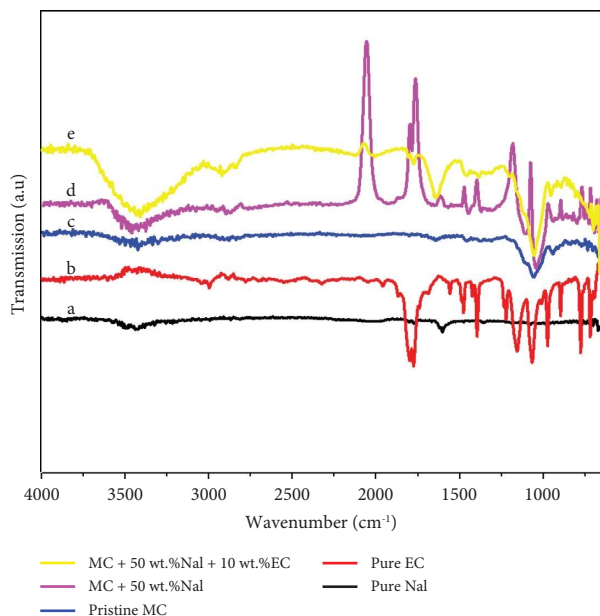

FIGURE 6: IR spectra of (a) NaI, (b) EC, (c) MC, (d) MC + 50 wt.% NaI, and (e) MC + 50 wt.% 10 wt.% EC.

compounds. A strong peak of C-O was observed at 1060 cm^{-1}, and the bending vibration of =C-H at 948 cm^{-1} suggested the presence of alcohol and alkenes, respectively. Two small bands of vibration were also observed at 1648 and 1376 cm^{-1}. Figure 6(d) shows the IR spectrum of the MC: NaI which features the interaction between MC and NaI. The

existence of a broad and strong peak observed at 3428 cm^{-1} corresponding to the O-H stretch and the C-H stretch of vibration at 2903 cm^{-1} indicated the existence of alcohols and alkanes, respectively. A strong band of C=O stretching at 1793 cm^{-1} and a medium band of =C-H observed at 1458 cm^{-1} were assigned to acid chlorides and aromatics, respectively. Two strong bands of C-O at 1380 and 1052 cm^{-1} were ascribed to alcohols. Finally, the two absorption peaks observed at 702 and 672 cm^{-1} corresponding to the vibration of C-H bending were assigned to aromatic compounds. The IR spectrum of the EC-based MC: NaI is shown in Figure 6(e) confirming the occurrence of vibration bands. The band of O-H stretching at 3428 cm^{-1} suggested the occurrence of alcohols. Two peaks of absorption were observed at 2918 and 2903 cm^{-1} both of C-H stretching referred to alkanes and alkyl groups. A strong band of C=O stretch observed at 1648 cm^{-1} and the C-H bending at 698 cm^{-1} is assigned to amide and aromatic compounds, respectively. The bending vibration of =C-H was observed at 695 cm^{-1} suggesting the existence of the alkenes. Four vibration peaks were also positioned at 2005, 1774, 1052, and 952 cm^{-1} in the spectrum of EC-doped MC: NaI. The changes in intensities of peaks and positions observed in the IR data of the MC: NaI complex and EC-based SPE were caused by phase and chemical composition changes. Some peaks initially present in the pure NaI salt are also found in MC: NaI with a shift in position and intensity. The additional peaks present in MC: NaI at 2903, 1793, 1458, 1380, 1052, 702, and 672 cm^{-1} confirmed the interaction between MC and NaI. About the connection of Na$^+$ ions to the C-O and

=C-H stretching of MC, the C-O stretching at 1060 cm^{-1} and the =C-H stretching at 948 cm^{-1} have changed to 1052 and 952 cm^{-1}, respectively, for the EC-based MC: NaI sample. It was found that some peaks (3428, 2903, and 1052 cm^{-1}) present in EC-based MC: NaI also appeared in MC: NaI. The existence of additional peaks in EC-based SPE indicated the interaction between NaI, EC, and MC, confirming the formation of a complex.

3.3. Analysis of AC Impedance.

The AC impedance method was used to study the electrical behavior of the SPE samples. Figure 7 depicts the Nyquist plots of pure MC, MC-NaI, and SPE films with EC amounts of 10, 20, 30, and 40 wt. % at RT. A semicircle and a spike may be seen in the high-frequency zone and the low-frequency region, respectively. The semicircle is created by the electrolyte's volume effect, and the spike occurs via the blocking effect of electrodes [46]. The intercept between the semicircle and the spike was used to compute the bulk electrolyte resistance of SPE. The addition of 50% NaI to MC lowered the diameter of the semicircle substantially, implying a drop in bulk resistance in NaI-based MC. The increase in the number of ionic charges induced by the addition of NaI could account for this decrease. The incorporation of different concentrations of EC into the MC: NaI matrix has also contributed to lowering bulk resistance, which may be related to increased polymer chain mobility. This decrease in semicircle diameter suggests an increase in σ. It should be noted that MC without salt has a σ value of roughly 3.1×10^{-11} S/cm, as computed from Figure 7(a). The σ value increases up to 3.02×10^{-3} S/cm after dispersing the salt in pure MC (Figure 7(b)), and the highest value of σ is found to be 5.06×10^{-3} S/cm for MC + 50 wt.% NaI + 10 wt% EC (SPE1), having the lowest R_b (Figure 7(c)).

3.3.1. Conductivity Measurements.

The conductivity σ was calculated at RT using equation (1). Table 2 shows the values of ionic conductivity for different concentrations of EC calculated at ambient temperature.

The highest σ value was determined with the sample SPE1: MC + 50 wt. %NaI + 10 wt.% EC. The variation in σ with the content of EC in the MC: NaI matrix is shown in Figure 8.

The addition of the optimal amount of 50 wt. % NaI in MC helps to raise σ of the MC from 3.1×10^{-11} to 3.02×10^{-3} S/cm. The inclusion of EC as a plasticizing agent into the MC: NaI matrix has also contributed to conductivity. The σ reaches a maximum value of 5.06×10^{-3} S/cm upon the incorporation of 10 wt. % EC. Figure 8 shows the conductivity trend in MC: NaI as a function of the EC concentration. The initial increase in the σ value was observed upon the addition of 10 wt. % EC. This increase was related to the increase in charge mobility due to the plasticizing effect of EC in the MC: NaI matrix, which decreases the glass transition temperature. The polymer chain loosened up, which contributed to reduced crystallinity and hence increased σ. The ion-association theory may be responsible for the further loss in conductivity at relatively high EC levels, which result in the development of ion
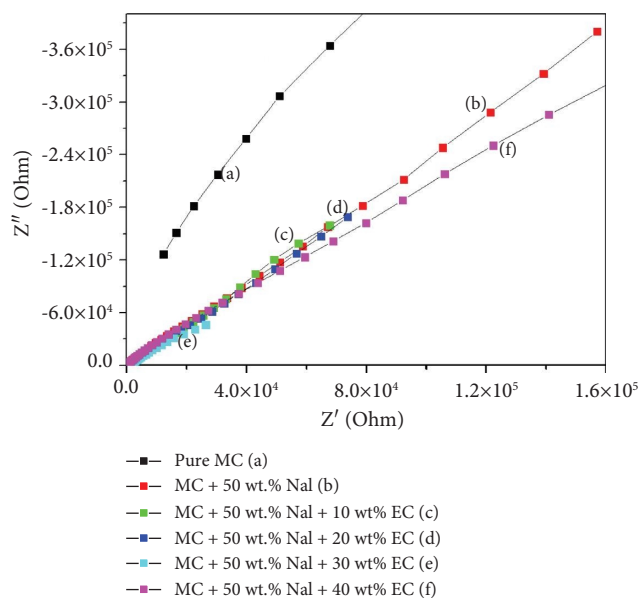

FIGURE 7: Nyquist plot for SPE samples: (a) pure MC, (b) SPE0, (c) SPE1, (d) SPE2, (e) SPE3, and (f) SPE4 at room temperature.

TABLE 2: Calculated RT-σ values of the prepared SPE films.

Samples	Ionic conductivity σ (S/cm^{-1})
Pure MC	3.10×10^{-11}
SPE0	3.02×10^{-3}
SPE1	5.06×10^{-3}
SPE2	1.00×10^{-3}
SPE3	2.45×10^{-3}
SPE4	9.09×10^{-4}

clusters and a decrease in carrier density. The Na$^+$ ions were entirely solvated by the solvent molecules by direct coordination of the solvent molecules with CO$_3^{2-}$ anions, which produced complicated ion-pair complexes. The redissociation of ion clusters was attributed to a further rise in σ value up to 2.45×10^{-3} S/cm at the high concentration of 30 wt% EC, which was due to the nearly high ε of the entire material, particularly that of the EC, which became dominant as the volume of EC content increased. This redissociation of ion clusters increased the carrier density, enhancing σ in SPE. Nevertheless, the carrier density has a significant impact on σ [47–49]. The redissociation of ion aggregates (clusters) was attributed to a subsequent rise in conductivity up to 2.45×10^{-3} S/cm^{-1} at a high level of 30 wt. % EC, which was due to the whole material's comparatively high dielectric constant, especially because of the EC, which became predominant as the quantity of the EC rose. The redissociation of ion aggregates enhanced the carrier density of mobile charges, resulting in improved SPE conductivity. The formation of ion-pair complexes as a result of direct interaction between EC, NaI, and MC resulted in the multiplication of free charges. This salvation led to a wide distribution of Na$^+$, CO$_3^{2-}$, and I$^-$, leading to improved σ at 30 wt. % IL. The introduction of more than 30 wt.% EC reduced free-charge mobility, which could have resulted in
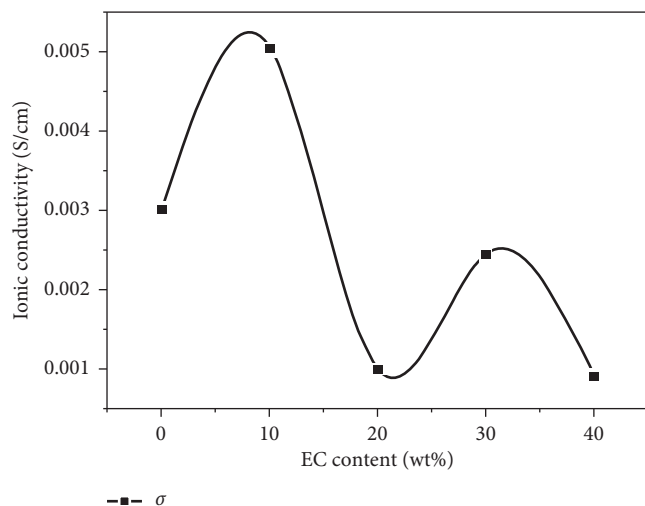
FIGURE 8: Variation of σ with the incorporation of EC in SPE: MC + 50 wt. % NaI.

ion aggregates. The creation of ion clusters slowed mobility and lowered the density of free ions, resulting in a drop in the σ value [50–55]. At lower concentrations, EC acts as a plasticizer by improving the mobility of the polymer chain which leads to an enhanced σ but a high concentration of EC in the SPE induced the formation of more nonconducting ions which do not contribute to the conductivity.

3.3.2. Dielectric Constant. Figure 9 depicts the variation of dielectric constant (ε) as a function of EC content in the MC: NaI system at 10^3 Hz. It is clear that ε and σ have the same trend and are both correlated to the concentration of carriers. The first increase in ε was due to the augmentation in carrier density, and the subsequent decline was caused by the blocking layer effect which accumulates the clusters in SPE and limits the formation of ion-pair complexes. The intermediate increase of 30 wt. % EC is because of the space-charge-induced enhancement effect, which speeds up conductor ions and boosts σ. The final fall in dielectric constant was related to the accumulation of a high number of ion clusters that slowed down the mobility of the polymer chain and which do not participate in σ. The ε-value for each EC concentration in the MC: NaI matrix was computed via equations (2)–(4). Table 3 summarizes the values of ε for each content of EC in the SPE calculated at 10^3 Hz.

3.3.3. Carrier Density and Mobility. Figure 10 shows the dependence of carrier density and mobility on EC amount in MC: NaI at RT. It has been seen that carrier concentration and mobility are at odds with one another. The initial rise in the carrier density upon the incorporation of 10% EC, followed by an increase up to 40% EC, is due to the increase of ion-pair complexes in the MC: NaI system, which increases conductivity. The 20 wt. % drop is due to ion agglomerations, which do not contribute to conductivity. The excessive number of ion clusters in the polymer blend matrix
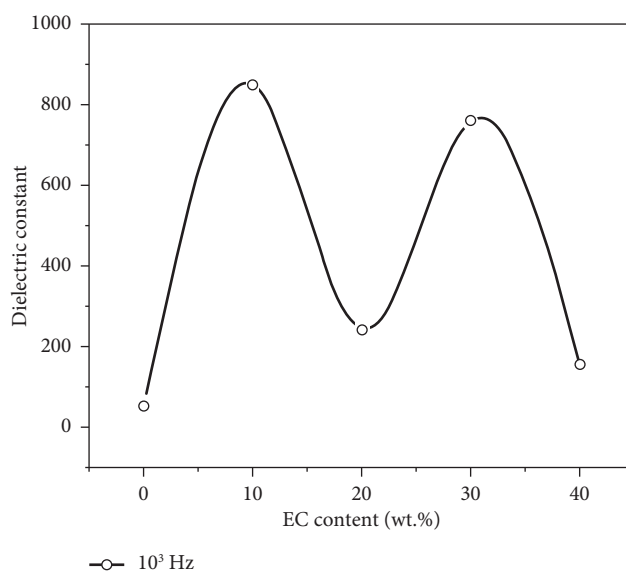

FIGURE 9: Dependence of ε with EC concentration in MC + 50 wt. % NaI system at 10^3 Hz.

TABLE 3: Dielectric constant values in polymer salt-complex with each amount of EC at frequency 10^3 Hz.

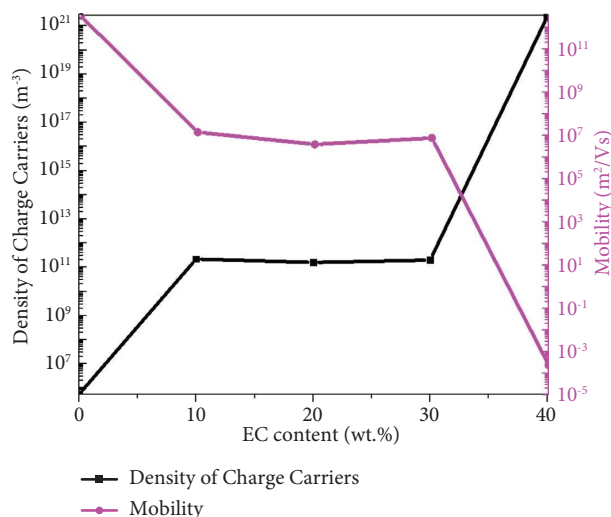| Samples	Dielectric constant (ε)
SPE0	52.63
SPE1	850.33
SPE2	241.46
SPE3	760.83
SPE4	155.89

FIGURE 10: The variation of carrier density and mobility with the amount of EC in the MC + 50 wt. % NaI system.

causes a reduction in carrier density at high EC content. At reduced salt concentrations, a limited quantity of carrier charges in the matrix allows the polymer chain to move more freely, enhancing its mobility. At high concentrations, salt in the MC + 50 wt.% NaI matrix works as an ion source

and as a plasticizer at lower concentrations, improving chain flexibility. The carrier concentration, on the other hand, monitors σ. The carrier density and mobility in SPE systems at RT are estimated using equations (5) and (6) and are shown in Table 4.

3.4. LSV Method.

The electrochemical stability window (ESW) of PE was found to be +1.50 to −1.0 V. The figure depicts the linear sweep voltammetry of the highest conducting polymer electrolytes, respectively. The electrochemical stability value for the highest conducting EC-incorporated SPE sample is found to be 2.5 V. The ESW was calculated using the prepared SPE sandwiched between two SS plates. Figure 11 depicts the LSV data of the optimal sample: MC + 50 wt. %NaI + 10 wt. %EC performed at a scan rate of 100 mV/s over the range [−3, 3 V]. The SPE's anodic voltammetry sweep revealed an oxidation onset at 1 V and a reduction onset at 1.5 V. There is no anodic current observed up to 0.975 V, implying that the SPE film does not undergo any electrochemical reaction in this region. When the electrode potential exceeds 1 V, the current gradually increases. This rise was caused by the degradation of the electrolyte sample [56]. For protonic polymer electrolytes and aqueous electrolytes, the typical potential window is approximately 1 V [57]. The obtained result indicates that the prepared SPE is thought to be suitable for energy storage device applications.

3.5. Transference Number Measurements.

Wagner's polarization technique was performed to verify both ion and electron contribution in the highly conductive PE. A voltage of 0.8 V was applied to induce polarization in the cell holding the optimal PE film: MC + 50 wt.% NaI + 10 wt.% EC. Figure 12 displays the current as a function of time. The curve drops steadily until it attains its I_{ss} value ($I_{ss} = 5.509 \times 10^{-7}$ A). The total current ($I_t = 5.527 \times 10^{-5}$ A) takes both contributions (ions and electrons) into consideration at the SS/SPE contact. I_{ss} confirms the cell's polarization caused by the blocking effect of the SS plates, but only electrons can travel through [58–60]. Using equations (7) and (8), the computed values of t_{ion} and t_{elec} which define the ion and electron contribution were found to be 99% and 1%, respectively. Because the contribution of electrons is so small, this result clearly shows that ions monitor conductivity.

3.6. CV Analysis.

The CV technique was used to test the supercapacitor's performance throughout a range of 0-1 V. Figure 13 depicts the manufactured device's capacitive behavior, revealing the supercapacitor's hysteresis buckle. A non-Faradaic mechanism during charge storage is suggested by the absence of a redox peak, establishing the existence of the supercapacitor [61]. To evaluate the capacitance response of the produced SC, the CV graphs were obtained at various scan rates ranging from 5–100 mV/s^{-1}. The CV curves were obtained from the SC with GO electrodes in a three-electrode configuration from 0 to 1 V using high-ionic

TABLE 4: The carrier density and mobility values for various EC contents in the MC + 50 wt. % NaI system.

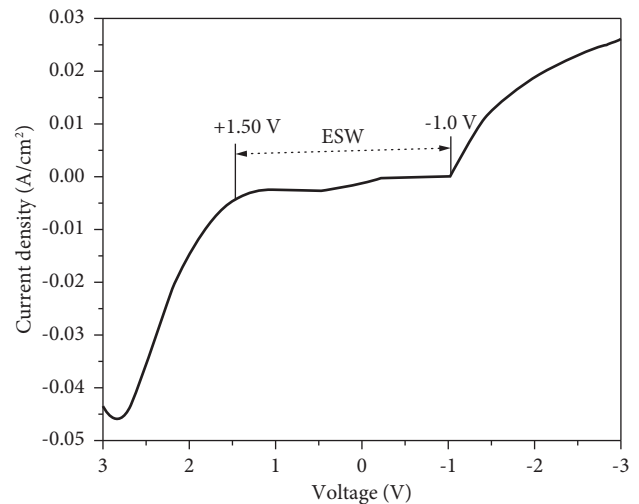| EC content (wt. %)	Carrier density (m^{-3})	Mobility (m^2/Vs)
0	5.50×10^5	3.43×10^{12}
10	2.19×10^{11}	14.44×10^6
20	1.58×10^{11}	3.95×10^6
30	1.97×10^{11}	7.77×10^6
40	2.39×10^{21}	2.37×10^{-4}

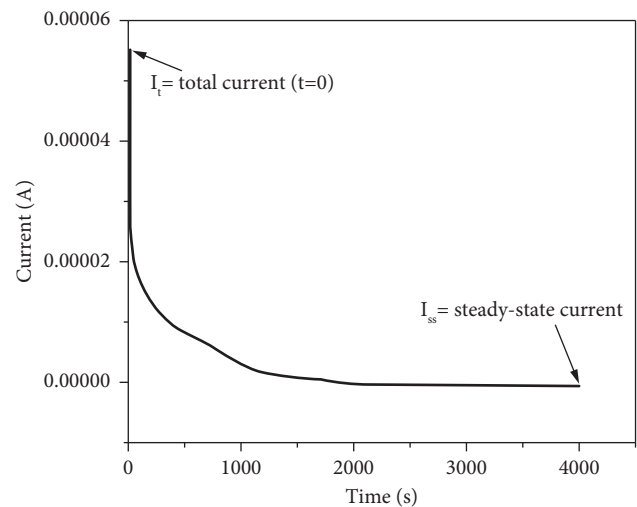FIGURE 11: LSV graph for the sample: MC + 50 wt. % NaI + 10 wt.% NaI at scan rate 100 mV/s at RT.

FIGURE 12: Time-dependent polarization current for the optimal SPE sample recorded at RT.

conductivity SPE. The electric field, which retains the ions of the electrolyte and polarizes the electrons of the electrode, charges the supercapacitor. The CV graphs were plotted to evaluate the performance of the device. The C_{sp} value of the EDLC was calculated from the CV graph using equation (9) and was 66.50 F/g. For the entire SC, the CV curves show typical quadratic CV profiles with a symmetric charge and discharge direction, suggesting EDLC behavior with a small
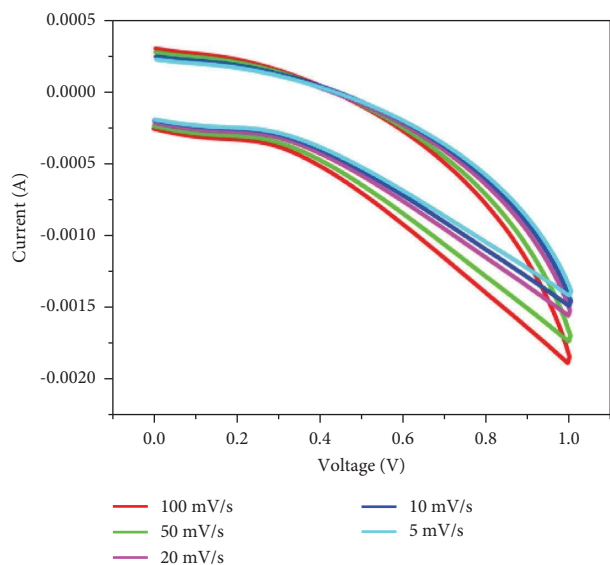
FIGURE 13: The optimized PE film-based supercapacitor's CV plot was obtained at different scan rates of 5–100 mV/s over 0-1 V.

Faraday contribution for charge storage. For all CV curves above 0.8 V, there was a significant deviation from the EDLC rectangular shape. The CV plots show that the total capacitance is distributed between 0 and 1 V for the best SPE sample, demonstrating the significance of the surface area and a narrow pore dispersion. According to the CV results, the symmetric device provided EDLC-dominant features with minor Faradaic contributions.

The electrochemical properties of the EDLC device can thus be considered good when considering its effectiveness in cyclability, as shown in Figure 14 with 10 cycles.

3.7. GCD Analysis.
The GCD graph of the EDLC manufactured with GO-based graphite sheets was analyzed. The coulomb efficiency of the GO-based system is computed using equation (10) and found to be 100%, indicating that the device can provide a load over an extended period. Figure 15 shows typical GCD curves of GO-3 electrodes at different current densities. The nearly symmetrical triangular curve represents typical capacitive behavior and good reversibility, and its intrinsic capacitance can be calculated according to equation (11). A fixed current density is applied to measure the potential of time. A voltage drop is noticed, suggesting that internal resistance exists in the structure. The linear charge/discharge curve demonstrates the capacitor behavior of the construction with a reduced Faradic process and low ESR value. The value of C_{sp} was estimated from the GCD curve and found to be 50 F·g^{-1} for a half-cell at 0.05 A·g^{-1}.

3.8. EIS Approach.
EIS is a valuable approach for studying ionic transport, bulk electrolyte characteristics, behavior of electrode-electrolyte interface, and other phenomena. EIS tool was used to investigate the effects of several factors on device performance, including charge-transfer resistance
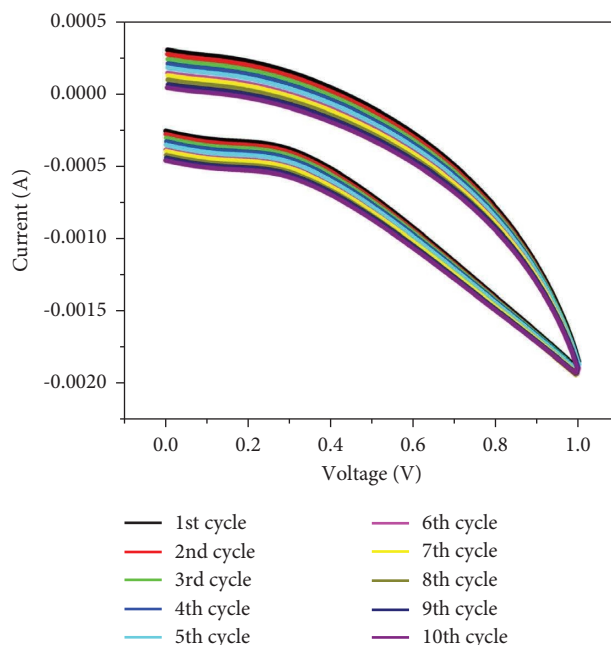

FIGURE 14: Cyclic voltammetry of the supercapacitor obtained at a scan rate of 10 mV/s^{-1} over 0-1 V, for ten first cycles.
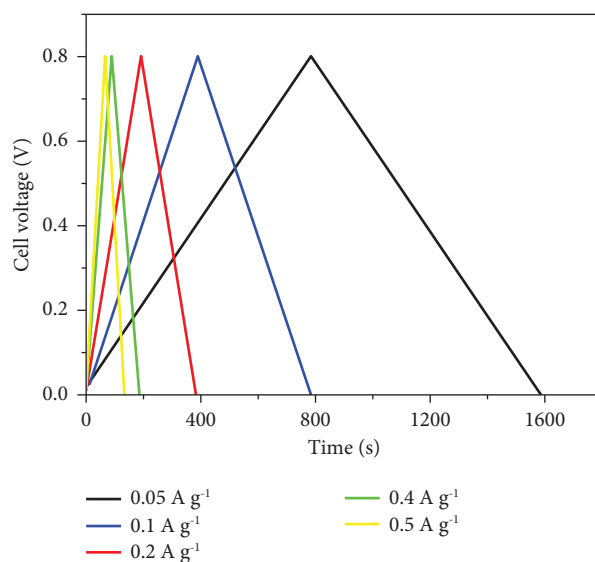

FIGURE 15: Charge-discharge curve for EDLC with the optimum PE at RT for different current densities.

(R_{ct}), bulk electrolyte resistance (R_s), and double-layer capacitance (C_{dl}) at low frequencies. Figure 16 depicts the impedance spectroscopy data for the supercapacitor cell obtained experimentally at low frequencies and a fitting plot of the equivalent electrical circuit (EEC) across the frequency range 0.1 MHz to 0.001 Hz using the optimal SPE: MC + 50 wt.% NaI + 10 wt.% EC. The Nyquist plot was simulated using the modified Randal's equivalent circuit [62, 63] that includes R_s, constant phase (Q) or C_{dl}, R_{ct}, and Warburg component (W), as shown in Figure 16. Basically, R_s and Z_w represent the bulk properties of the electrolyte solution and diffusion, whereas Q and R_{ct} are affected by the dielectric and
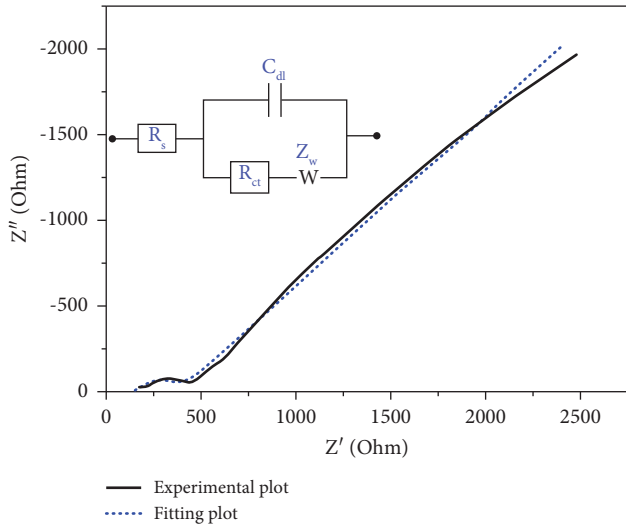
FIGURE 16: Fitting plot of experimental impedance and EEC for the optimized SPE: MC + 50 wt.% NaI + 10 wt. % EC.

TABLE 5: Obtained parameter values generated from fit data in origin pro 8.0 using the extrapolating graph approach [51].

Parameters (unit)	Value
R_s (Ω)	90.5
R_{ct} (Ω)	373
C_{dl} (μF)	6.7×10^{-5}
W ($\Omega \cdot s^{-1/2}$)	16.5×10^{-4}
$-Z''$ (Ω)	1711
C_{sp} (F$\cdot$g^{-1})	154.66

insulating characteristics at the interface between electrode and electrolyte. The capacitance between the electrolyte's ionic species and the electronic charges at the electrode surfaces is represented by C_{dl} in a parallel relationship with R_{ct} [64]. The Nyquist plot assists in determining R_{ct}. The standard Nyquist plot has a semicircular component that corresponds to the restricted process of electron transfer at high frequencies and a linear portion that corresponds to the constrained step of electrochemical diffusion at low frequencies [64]. The relative error of fitting was 0.5. The capacitance of a half-cell was calculated using the relationship (12) at 1 MHz and found to be 77.33 F$\cdot$g^{-1}. Table 5 presents various parameters obtained by fitting the EIS data using EEC.

An unplasticized MC-based electrolyte (75 wt% MC-25 wt% NH_4NO_3) with a conductivity of 2.10×10^{-6} S$\cdot$cm^{-1} yields a low capacity of 1-2 F$\cdot$g^{-1} when used in a capacitor, according to prior work [65]. The complex CS: DN: NH_4I: Zn (II) was plasticized with different concentrations of glycerol (GL), and the effects of the metal complex and GL on the properties of the generated electrolyte were investigated [66]. Because the solid SPE sample (MC + 50 wt.% NaI + 10 wt.% EC) has a conductivity of 5.06×10^{-3} S$\cdot$cm^{-1} (almost two orders of magnitude higher), the capacitance of the resulting EDLC should be higher (154.66 F$\cdot$g^{-1}). According to electrochemical impedance spectroscopy (EIS) studies, the plasticized system's greatest conductivity was 3.44×10^{-4} S/cm, which is one order of magnitude less than our current system. TNM data indicated that the transport mechanism in the produced electrolyte is largely ionic, with a high value of $t_{ion} = 0.983$, which is less than the 0.99 achieved with the MC: NaI: EC system. The ESW of the CS: DN: NH_4I: Zn (II) electrolyte was determined to be 1.25 V using LSV data. This value is found to be less than 2.5 V obtained with the LSV method for the MC-based system developed in this work. Shujahadeen B. et al. developed MC: Dextran (Dex) polymer blend electrolytes containing NH_4I salt for EDLC application [67]. The highest conductivity is determined to be 1.12×10^{-3} S/cm for 40% NH_4I, which is lower than that of the MC-NaI: EC system. The LSV investigation demonstrated that the MC: Dex: NH_4I electrolyte has an ESW value of 1.27 V, which is lower than 2.5 V for the optimum sample: MC + 50 wt. % NaI + 10 wt. % EC.

The current study and prior studies emphasize the importance of biopolymers in polymer electrolyte synthesis and device manufacturing. In emerging technologies, the need for flexible energy storage devices, such as EDLCs and batteries, drives researchers to create and discover new materials. Of course, one concern in this industry is that biopolymer-based devices are not resistant to higher cycle numbers. Table 5 summarizes several essential parameters that can contribute to enhanced device performance. First, selecting the suitable polymer, which is one of the crucial elements, is significantly important in achieving optimum performance. In EDLC applications, the pristine polymer should have good ionic conduction as well as excellent chemical, thermal, and mechanical stability. These characteristics provide the manufactured EDLC device with good outputs and long cyclability. Second, when using PE in electrochemical device applications, it is critical to choose an adequate dopant salt. Salts with low lattice energy are easily dissociated, but salts with high lattice energy cannot be dissolved by the host medium alone, resulting in a free carrier dilemma. Furthermore, the use of plasticizers can promote ionic conduction; however, substantial quantities might cause physical instability and enhance sensitivity to electrodes. Our research group is working to create PE films with high conductivity and improve device performance. As truthful as possible, all biopolymer-based outcomes should be published to the benefit of researchers to shed light on the advances made in this sector. These findings indicate that high-performance gadgets will be built in future endeavors. Nevertheless, further attention from scientists is required. Biopolymer-based devices must be prioritized since they are completely nontoxic and do not include any harmful components. As previously stated, numerous aspects such as functional groups of the polymer chain backbone, salt lattice energy, and plasticizers influence device performance. As a result, various polymers, salts, or plasticizers should be researched, and their findings should be presented to the scientific world in the form of research publications. Nonetheless, the performance of biopolymer-based EDLC devices has been good thus far, and increased performance is predicted shortly. Table 6 displays the ionic conductivity (σ), ionic transference number (t_{ion}), and specific capacitance (C_{sp}) values obtained for the recently developed SPEs and the presently employed SPE.

TABLE 6: Summary of the values of σ, t_{ion}, and C_{sp} for recent SPE systems including the optimized SPE film: MC + 50 wt. % NaI + 10 wt. % EC.

Samples	σ (S/cm^{-1})	t_{ion}	C_{sp} (Fg^{-1})	References
PVA-MC-NH$_4$I	7.01×10^{-8}	0.964	—	[65]
MC-NH$_4$F	6.40×10^{-7}	—	—	[66]
MC-NH$_4$NO$_3$	2.10×10^{-6}	—	1-2	[67]
MC-NaI	2.70×10^{-5}	—	—	[68]
CS: DN: NH$_4$I: Zn (II)	3.44×10^{-4}	0.983	108.3	[69]
MC-KI-glycerol	5.14×10^{-4}	0.964	68	[70]
CS: MC: NH$_4$I	6.65×10^{-4}	0.97	9-10	[71]
MC: Dex: NH$_4$I	1.12×10^{-3}	0.98	79	[30]
NaCMC/PVA	2.25×10^{-3}	0.99	—	[29]
MC-NaI: EC	5.06×10^{-3}	0.99	154.66	This work

4. Conclusions

New flexible SPE, made of MC, NaI, and EC, used as a plasticizer to increase conductivity were successfully created using the solution cast technique. FTIR findings revealed the creation of a complex between MC, NaI, and EC following the addition of NaI and EC, which modified the chemical composition of the entire electrolyte. This conclusion was also supported by POM data, which revealed a change in the surface morphology of the matrix as a consequence of the salt and plasticizer impact and the creation of the amorphous phase. EIS data revealed a considerable decrease in bulk resistance as a result of metal complex dispersion, which boosted conductivity. The improved SPE's ionic conductivity was found to be two orders of magnitude more than that of MC-NaI and some other results were reported above. The highly conductive electrolyte sample exhibited outstanding electrochemical stability, which would be essential for protonic devices because of standard potential value as 1 V. The supercapacitor device was designed and tested using the optimized SPE film. The device demonstrated an excellent linear charge/discharge behavior, and the system delivers the charge over an extended period. The inclusion of EC in MC-NaI has not only contributed to increasing σ but also increased the flexibility of the SPE which improved its properties. The GO-electrode's porous structure that interacts with the EC-based MC-NaI electrolyte limited equivalent series resistance (ESR) which limits the capacity loss due to the effect of the plasticizer (EC) at the interface. The low capacitance of the device may be related to the limited number of micropores present on the electrode surface of GO, which contributes to an increase in capacitance. According to the results reported in this work, novel gel electrolytes are solid and flexible, with high electrochemical stability properties that prevent leakage, increase safety features, and workability, which are necessary for good solid-state EDLC devices and storage batteries.

Data Availability

The data used to support the findings of this study are available from the corresponding author upon request.

Disclosure

Theodore Azemtsop Manfo received the B.S. and M.S. degrees in physics from the University of Yaounde I, in 2015, and the Ph.D. degree in Physics from Sharda University, Greater Noida, Uttar Pradesh, India, in 2021. Since 2016, he has been a lecturer at the Department of Physics, Laboratory of Material Science at the University of Yaounde I. After his doctorate, he worked as a Postdoctoral Researcher at Sharda University in India from 2021-22. He is now a Visiting Researcher at Recep Tayyip Erdogan University, Rize, Turkey, in the Department of Electrical and Electronic Engineering. He is the author of one book, many research articles, and one applied patent. His research interests include solid/ gel polymer electrolytes, ionic liquids, electrode materials (GO, AC, and CNT), supercapacitors, batteries, PV systems, hybrid systems, manufacture and characterization of materials for energy storage and conversion, and electrochemical devices. After his Ph.D., he carried out two projects and published high-quality research papers such as (1) Badi, N.; Theodore, A.M.; Alghamdi, S.A.; Al-Aoh, H.A.; Lakhouit, A.; Roy, A.S.; Alatawi, A.S.; Ignatiev, A. Fabrication and Characterization of Flexible Solid Polymers Electrolytes for Supercapacitor Application. Polymers 2022, 14, 3837. https://doi.org/10.3390/polym14183837; (2) Badi, N.; Theodore, A.M.; Alghamdi, S.A.; Al-Aoh, H.A.; Lakhouit, A.; Singh, P.K.; Norrrahim, M.N.F.; Nath, G. The Impact of Polymer Electrolyte Properties on Lithium-Ion Batteries. Polymers 2022, 14, 3101. https://doi.org/10.3390/polym14153101; (3) Badi N, Theodore AM, Alghamdi SA, Alatawi AS, Almasoudi A, Lakhouit A, et al. (2022) Thermal effect on curved photovoltaic panels: Model validation and application in the Tabuk region. PLoS ONE 17 (11): e0275467. https://doi.org/10.1371/journal.pone.0275467. He also published a book called 'The Impact of Polymer Electrolyte Properties on Lithium-Ion Batteries (Bulevarddul Moscova 21, Chisinau, Moldova, Eliva Press Global Ltd. part of Eliva Press S.R.L, 2022). He is currently working on electrical and electronic hybrid systems combining supercapacitors, batteries, and PV systems for industrial applications with Ass. (Prof.) Dr. Mustafa Ergin Şahin and Prof. Dr. Fahri Eyüp Fahri Keskenler.

Conflicts of Interest

The author declares that there are no conflicts of interest.

Acknowledgments

References

[1] D. E. Fenton, J. M. Parker, and P. V. Wright, "Complexes of alkali metal ions with poly (ethylene oxide)," *Polymer*, vol. 14, pp. 589–11, 1973.

[2] C. C. Sun, A. H. You, and L. L. Teo, "Characterizations of PMMA-based polymer electrolyte membranes with Al2O3,"

Journal of Polymer Engineering, vol. 39, no. 7, pp. 612–619, 2019.

[3] L. O. Faria and R. L. Moreira, "Dielectric behavior of P(VDF-TrFE)/PMMA blends," *Journal of Polymer Science Part B: Polymer Physics*, vol. 37, pp. 2996–3002, 1999.

[4] C.-S. Liao and W.-B. Ye, "Enhanced ionic conductivity in poly(ethylene oxide)/layered double hydroxide nanocomposite electrolytes," *Journal of Polymer Research*, vol. 10, no. 4, pp. 241–246, 2003.

[5] B. Liang, S. Tang, Q. Jiang et al., "Preparation and characterization of PEO-PMMA polymer composite electrolytes doped with nano-Al2O3," *Electrochimica Acta*, vol. 169, pp. 334–341, 2015.

[6] D. Lin, W. Liu, Y. Liu et al., "High ionic conductivity of composite solid polymer electrolyte via in situ synthesis of monodispersed SiO2 nanospheres in poly(ethylene oxide)," *Nano Letters*, vol. 16, no. 1, pp. 459–465, 2015.

[7] P. Pal and A. Ghosh, "Investigation of ionic conductivity and relaxation in plasticized PMMA-LiClO4 solid polymer electrolytes," *Solid State Ionics*, vol. 319, pp. 117–124, 2018.

[8] Q. Chenying, H. Zhaoxia, W. Xiaohui, W. Jian, W. Kai, and L. Siyao, "Research progress of gel polymer electrolytes on solid supercapacitors," *Energy Storage Science and Technology*, vol. 9, no. 3, pp. 776–783, 2020.

[9] A. Manfo T, S. Konwar, P. K. Singh, R. M. Mehra, Y. Kumar, and M. Gupta, "PEO + NaSCN and ionic liquid based polymer electrolyte for supercapacitor," *Materials Today: Proceedings*, vol. 34, pp. 802–812, 2021.

[10] S. Ahmad, "Retracted article: polymer electrolytes: characteristics and peculiarities," *Ionics*, vol. 15, no. 3, pp. 309–321, 2009.

[11] W. H. Meyer, "Polymer electrolytes for lithium-ion batteries," *Advanced Materials*, vol. 10, no. 6, pp. 439–448, 1998.

[12] N. Badi, A. M. Theodore, S. A. Alghamdi et al., "The impact of polymer electrolyte properties on lithium-ion batteries," *Polymers*, vol. 14, pp. 3101–15, 2022.

[13] Y. Kumar and M. Gupta, "Physical characterization of ionic liquid-modified polyvinyl alcohol and sodium thiocyanate polymer electrolytes for electrochemical double-layer capacitor application," *Journal of Shanghai Jiaotong University*, vol. 28, no. 2, 2021.

[14] M. Premalatha, N. Vijaya, S. Selvasekarapandian, and S. Selvalakshmi, "Characterization of blend polymer PVA-PVP complexed with ammonium thiocyanate," *Ionics*, vol. 22, no. 8, pp. 1299–1310, 2016.

[15] B. Nacer, S. A. Alghamdi, A. Hatem et al., "Fabrication and characterization of flexible solid polymers electrolytes for supercapacitor application," *Polymers*, vol. 14, pp. 3837–18, 2022.

[16] V. Bharti, P. K. Singh, and J. P. Sharma, "Development of polymer electrolyte membranes based on biodegradable polymer," *Materials Today: Proceedings*, vol. 34, pp. 856–862, 2021.

[17] N. E. A. Shuhaimi, L. P. Teo, S. R. Majid, and A. K. Arof, "Transport studies of NH4NO3 doped methyl cellulose electrolyte," *Synthetic Metals*, vol. 160, no. 9–10, pp. 1040–1044, 2010.

[18] M. T. Taghizadeh and P. Seifi-Aghjekohal, "Sonocatalytic degradation of 2-hydroxyethyl cellulose in the presence of some nanoparticles," *Ultrasonics Sonochemistry*, vol. 26, pp. 265–272, 2015.

[19] M. Fadhlullah and A. Shukur, *Characterization of ion conducting solid biopolymer electrolytes based on starch-chitosan blend and application in electrochemical devices*, Ph.D. thesis, University of Malaya, Kuala Lumpur, Malaysia, 2015.

[20] C. Chotsuwan, S. Boonrungsiman, U. Asawapirom et al., "Highly viscous composite gel electrolyte based on cellulose acetate and nanoparticles," *Journal of Electroanalytical Chemistry*, vol. 828, pp. 91–96, 2018.

[21] A. T. Manfo, P. K. Singh, R. M. Mehra, R. C. Singh, and M. Gupta, "Structural, vibrational, electrical, electrochemical and capacitive investigations on ionic liquid doped P (VDF-HFP) + NaSCN based polymer electrolytes," *Recent Innovations in Chemical Engineering (Formerly Recent Patents on Chemical Engineering)*, vol. 14, pp. 21–34, 2021.

[22] M. A. Brza, S. B. Aziz, H. Anuar et al., "Metal framework as a novel approach for the fabrication of electric double layer capacitor device with high energy density using plasticized poly(vinyl alcohol): ammonium thiocyanate based polymer electrolyte," *Arabian Journal of Chemistry*, vol. 13, no. 10, pp. 7247–7263, 2020.

[23] S. A. Alexandre, G. G. Silva, R. Santamaría, J. P. C. Trigueiro, and R. L. Lavall, "A highly adhesive PIL/IL gel polymer electrolyte for use in flexible solid state supercapacitors," *Electrochimica Acta*, vol. 299, pp. 789–799, 2019.

[24] M. H. Hamsan, M. F. Shukur, and M. F. Z. Kadir, "NH4NO3 as charge carrier contributor in glycerolized potato starch-methyl cellulose blend-based polymer electrolyte and the application in electrochemical double-layer capacitor," *Ionics*, vol. 23, no. 12, pp. 3429–3453, 2017.

[25] S. B. Aziz, M. H. Hamsan, R. M. Abdullah, and M. F. Z. Kadir, "A promising polymer blend electrolytes based on chitosan: methyl cellulose for EDLC application with high specific capacitance and energy density," *Molecules*, vol. 24, pp. 2503–13, 2019.

[26] S. B. B Aziz, M. H. H Hamsan, M. M. M Nofal et al., "From cellulose, shrimp and crab shells to energy storage EDLC cells: the study of structural and electrochemical properties of proton conducting chitosan-based biopolymer blend electrolytes," *Polymers*, vol. 12, no. 7, p. 1526, 2020.

[27] C. V. Subba Reddy, A. P. Jin, Q. Y. Zhu, L. Q. Mai, W. Chen, and W. Chen, "Preparation and characterization of (PVP + NaClO4) electrolytes for battery applications," *The European Physical Journal E*, vol. 19, no. 4, pp. 471–476, 2006.

[28] A. M. Abdullah, S. B. Aziz, and S. R. Saeed, "Structural and electrical properties of polyvinyl alcohol (PVA): methyl cellulose (MC) based solid polymer blend electrolytes inserted with sodium iodide (NaI) salt," *Arabian Journal of Chemistry*, vol. 14, pp. 103388–11, 2021.

[29] V. Cyriac, I. M. N. Ismayil, I. M. Noor et al., "Ionic conductivity enhancement of PVA: carboxymethyl cellulose poly-blend electrolyte films through the doping of NaI salt," *Cellulose*, vol. 29, no. 6, pp. 3271–3291, 2022.

[30] S. B. Aziz, M. A. Brza, K. Mishra et al., "Fabrication of high performance energy storage EDLC device from proton conducting methylcellulose: dextran polymer blend electrolytes," *Journal of Materials Research and Technology*, vol. 9, no. 2, pp. 1137–1150, 2020.

[31] S. B. Aziz and Z. H. Z. Abidin, "Ion-transport study in nanocomposite solid polymer electrolytes based on chitosan: electrical and dielectric analysis," *Journal of Applied Polymer Science*, vol. 132, 15 pages, 2014.

[32] H. J. Schütt and E. Gerdes, "Space-charge relaxation in ionically conducting glasses. II. Free carrier concentration and mobility," *Journal of Non-crystalline Solids*, vol. 144, pp. 14–20, 1992.

[33] R. T. Abdulwahid, S. B. Aziz, M. A. Brza et al., "Electrochemical performance of polymer blend electrolytes based on chitosan: dextran: impedance, dielectric properties, and energy storage study," *Journal of Materials Science: Materials in Electronics*, vol. 32, no. 11, pp. 14846–14862, 2021.

[34] S. B. Aziz, M. H. Hamsan, W. O. Karim et al., "Study of impedance and solid-state double-layer capacitor behavior of proton (H+)-Conducting polymer blend electrolyte-based CS: PS polymers," *Ionics*, vol. 26, no. 9, pp. 4635–4649, 2020.

[35] G. P. Pandey, Y. Kumar, and S. A. Hashmi, "Ionic liquid incorporated PEO based polymer electrolyte for electrical double layer capacitors: a comparative study with lithium and magnesium systems," *Solid State Ionics*, vol. 190, no. 1, pp. 93–98, 2011.

[36] S. B. Aziz, M. G. Faraj, and O. G. Abdullah, "Impedance spectroscopy as a novel approach to probe the phase transition and microstructures existing in CS: PEO based blend electrolytes," *Scientific Reports*, vol. 8, no. 1, Article ID 14308, 2018.

[37] X. Huang, T. Ren, L. Tian, L. Hong, W. Zhu, and X. Tang, "Morphology and ionic conductivity of solid polymer electrolytes based on polyurethanes with various topological structures," *Journal of Materials Science*, vol. 39, no. 4, pp. 1221–1225, 2004.

[38] S. B. Aziz and R. M. Abdullah, "Crystalline and amorphous phase identification from the tanδ relaxation peaks and impedance plots in polymer blend electrolytes based on [CS: AgNt]x:PEO(x-1) (10 ≤ x ≤ 50)," *Electrochimica Acta*, vol. 285, pp. 30–46, 2018.

[39] G. Jo, H. Ahn, and M. J. Park, "Simple route for tuning the morphology and conductivity of polymer electrolytes: one end functional group is enough," *ACS Macro Letters*, vol. 2, pp. 990–995, 2013.

[40] M. F. Shukur, R. Ithnin, and M. F. Z. Kadir, "Electrical properties of proton conducting solid biopolymer electrolytes based on starch–chitosan blend," *Ionics*, vol. 20, no. 7, pp. 977–999, 2013.

[41] S. B. Aziz, S. Al-Zangana, H. J. Woo, M. F. Z. Kadir, and O. G. Abdullah, "The compatibility of chitosan with divalent salts over monovalent salts for the preparation of solid polymer electrolytes," *Results in Physics*, vol. 11, pp. 826–836, 2018.

[42] M. H. Buraidah and A. K. Arof, "Characterization of chitosan/PVA blended electrolyte doped with NH4I," *Journal of Non-crystalline Solids*, vol. 357, no. 16–17, pp. 3261–3266, 2011.

[43] M. N. Chai and M. I. N. Isa, "Electrical characterization and ionic transport properties of carboxyl methylcellulose-oleic acid solid polymer electrolytes," *International Journal of Polymer Analysis and Characterization*, vol. 18, no. 4, pp. 280–286, 2013.

[44] S. N. Bhad and V. S. Sangawar, "Optical study of PVA-based gel electrolyte," *International Journal of Scientific Engineering and Research*, vol. 4, no. 6, p. 1719, 2013.

[45] M. A. Saadiah, Y. Nagao, and A. S. Samsudin, "Enhancement on protonation (H+) with incorporation of flexible ethylene carbonate in CMC–PVA–30 Wt % NH4NO3 film," *International Journal of Hydrogen Energy*, vol. 46, no. 33, pp. 17231–17245, 2021.

[46] L. Fan, Z. Dang, C. W. Nan, and M. Li, "Thermal, electrical and mechanical properties of plasticized polymer electrolytes based on PEO/P(VDF-HFP) blends," *Electrochimica Acta*, vol. 48, pp. 205–209, 2002.

[47] P. B. Bhargav, V. M. Mohan, A. K. Sharma, V. V. R. N. Rao, and V. V. R. N. Rao, "Structural and electrical properties of pure and NaBr doped poly (vinyl alcohol) (PVA) polymer electrolyte films for solid state battery applications," *Ionics*, vol. 13, no. 6, pp. 441–446, 2007.

[48] N. A. Nik Aziz, N. K. Idris, and M. I. N. Isa, "Solid polymer electrolytes based on methylcellulose: FT-IR and ionic conductivity studies," *International Journal of Polymer Analysis and Characterization*, vol. 15, no. 5, pp. 319–327, 2010.

[49] A. S. Samsudin, W. M. Khairul, and M. Isa, "Characterization on the potential of carboxy methylcellulose for application as proton conducting biopolymer electrolytes," *Journal of Non-crystalline Solids*, vol. 358, no. 8, pp. 1104–1112, 2012.

[50] N. S. Salleh, S. B. Aziz, Z. Aspanut, and M. F. Z. Kadir, "Electrical impedance and conduction mechanism analysis of biopolymer electrolytes based on methyl cellulose doped with ammonium iodide," *Ionics*, vol. 22, no. 11, pp. 2157–2167, 2016.

[51] S. Iqbal, H. Khatoon, A. Hussain Pandit, and S. Ahmad, "Recent development of carbon-based materials for energy storage devices," *Materials Science for Energy Technologies*, vol. 2, no. 3, pp. 417–428, 2019.

[52] L. Bach-Toledo, B. M. Hryniewicz, L. F. Marchesi, L. H. Dall'Antonia, M. Vidotti, and F. Wolfart, "Conducting polymers and composites nanowires for energy devices: a brief review," *Materials Science for Energy Technologies*, vol. 3, pp. 78–90, 2020.

[53] P. H. Maheshwari, "Developing the processing stages of carbon fiber composite paper as efficient materials for energy conversion, storage, and conservation," *Materials Science for Energy Technologies*, vol. 2, no. 3, pp. 490–502, 2019.

[54] P. M. Anjana, M. R. Bindhu, and R. B. Rakhi, "Green synthesized gold nanoparticle dispersed porous carbon composites for electrochemical energy storage," *Materials Science for Energy Technologies*, vol. 2, no. 3, pp. 389–395, 2019.

[55] S. R. Eedulakanti, A. K. Gampala, C. Shilpa Chakra, V. Gedela, R. Boddula, and K. Venkateswara Rao, "Ultrasonication assisted thermal exfoliation of graphene-tin oxide nanocomposite material for supercapacitor," *Materials Science for Energy Technologies*, vol. 2, no. 3, pp. 372–376, 2019.

[56] L. Sampathkumar, P. Christopher Selvin, S. Selvasekarapandian, P. Perumal, R. Chitra, and M. Muthukrishnan, "Synthesis and characterization of biopolymer electrolyte based on tamarind seed polysaccharide, lithium perchlorate and ethylene carbonate for electrochemical applications," *Ionics*, vol. 25, no. 3, pp. 1067–1082, 2019.

[57] R. Pratap, B. Singh, and S. Chandra, "Polymeric rechargeable solid-state proton battery," *Journal of Power Sources*, vol. 161, no. 1, pp. 702–706, 2006.

[58] C. Devi, J. Gellanki, H. . Pettersson, and S. Kumar, "High sodium ionic conductivity in PEO/PVP solid polymer electrolytes with InAs nanowire fillers," *Scientific Reports*, vol. 11, pp. 20180-20181, 2021.

[59] M. S. A. Rani, A. Ahmad, and N. S. Mohamed, "Influence of nano-sized fumed silica on physicochemical and electrochemical properties of cellulose derivatives-ionic liquid biopolymer electrolytes," *Ionics*, vol. 24, no. 3, pp. 807–814, 2017.

[60] M. Z. Kufian, M. F. Aziz, M. F. Shukur et al., "PMMA–LiBOB gel electrolyte for application in lithium ion batteries," *Solid State Ionics*, vol. 208, pp. 36–42, 2012.

[61] G. P. Pandey, Y. Kumar, and S. A. Hashmi, "Ionic liquid incorporated PEO based polymer electrolyte for electrical double layer capacitors: a comparative study with lithium and magnesium systems," *Solid State Ionics*, vol. 190, no. 1, pp. 93–98, 2011.

[62] G. Xu, C. Zheng, Q. Zhang et al., "Binder-free activated carbon/carbon nanotube paper electrodes for use in super-capacitors," *Nano Research*, vol. 4, no. 9, pp. 870–881, 2011.

[63] A. Di Fabio, A. Giorgi, M. Mastragostino, and F. Soavi, "Carbon-Poly(3-methylthiophene) hybrid supercapacitors," *Journal of the Electrochemical Society*, vol. 148, pp. L11–12, 2001.

[64] T. Manfo, K. Azemtsop, P. K. Singh, R. C. Singh, and R. M. Mehra, "Yogesh kumar, and meenal gupta. "WITHDRAWN: PVA + NaSCN and ionic liquid based polymer electrolyte for supercapacitor," *Materials Science for Energy Technologies*, 2020.

[65] M. M. Nofal, S. B. Aziz, M. A. Brza et al., "Studies of circuit design, structural, relaxation and potential stability of polymer blend electrolyte membranes based on PVA:MC impregnated with NH4I salt," *Membranes*, vol. 12, no. 3, p. 284, 2022.

[66] N. A. N. Aziz, N. K. Idris, and M. I. N. Isa, "Proton conducting polymer electrolytes of methylcellulose doped ammonium fluoride: conductivity and ionic transport studies," *International Journal of the Physical Sciences*, vol. 5, no. 6, pp. 748–752, 2010.

[67] N. E. A. Shuhaimi, S. R. Majid, and A. K. Arof, "On complexation between methyl cellulose and ammonium nitrate," *Materials Research Innovations*, vol. 13, no. 3, pp. 239–242, 2009.

[68] A. Zainal and J. Farghali, "Fourier transform infrared spectroscopy and electrical characterization of methylcellulose based solid polymer electrolyte doped with sodium iodide," *Jurnal Teknologi*, vol. 76, 3 pages, 2015.

[69] M. H. Hamsan, M. M. Nofal, S. B. Aziz et al., "Plasticized polymer blend electrolyte based on chitosan for energy storage application: structural, circuit modeling, morphological and electrochemical properties," *Polymers*, vol. 13, no. 8, p. 1233, 2021.

[70] S. B. Aziz, M. H. Hamsan, M. A. Brza, M. F. Z. Kadir, S. K. Muzakir, and R. T. Abdulwahid, "Effect of glycerol on EDLC characteristics of chitosan:methylcellulose polymer blend electrolytes," *Journal of Materials Research and Technology*, vol. 9, no. 4, pp. 8355–8366, 2020.

[71] S. Aziz, E. Dannoun, R. Abdulwahid et al., "The study of ion transport parameters in MC-based electrolyte membranes using EIS and their applications for EDLC devices," *Membranes*, vol. 12, no. 2, p. 139, 2022.